Electronic states in quasi-one-dimensional wires with nonuniform magnetic fields

Y. Takagaki and K. Ploog
Paul-Drude-Institut für Festkörperelektronik, Hausvogteiplatz 5-7, D-10117 Berlin, Germany
(Received 4 April 1995; revised manuscript received 16 October 1995)

We have investigated the transmission of an electron in quasi-one-dimensional systems in the presence of nonuniform magnetic fields. The subband energy and the wave function in a magnetic field, whose strength varies parabolically in the transverse direction, are calculated. This model is expected to describe a composite fermion in quantum wires. The parabolic magnetic field is found to increase the band-edge energies and modify the probability distribution significantly. When a moderate negative offset magnetic field is added, the subband energy takes a minimum value for a finite parabolic magnetic-field strength and the wave function of the lowest subband is double peaked. We have calculated magnetic-field dependencies of the bend resistance and the Hall resistance in a cross junction, in which the parabolic magnetic field is assumed. The positions in magnetic field of the peak in the bend resistance due to ballistic transport and of the zero Hall resistance are shifted and generally do not coincide as the parabolic field is imposed. We also examine the conductance of quantum wires in the presence of random magnetic fields. The nonuniform magnetic fields lead to universal conductance fluctuations in the metallic regime and to exponential decay of the conductance as the length is increased in the localized regime. In contrast to the impurity scattering case, the localization length is found to be smaller for larger average magnetic fields.

I. INTRODUCTION

Electron transport in nonuniform magnetic fields has attracted much attention in recent years.[1] It has been found that random magnetic fields lead to the localization of electronic states in quasi-one-dimensional (quasi-1D) systems.[2] The localization in two-dimensional (2D) systems in the presence of the random magnetic field with zero mean value is now under intensive investigation. The situtaion is closely related to the fractional quantum Hall state of the 2D electron gas at the filling factor $\nu=\frac{1}{2}$. The theory by Halperin, Lee, and Read[3] predicts near $\nu=\frac{1}{2}$ the presence of a certain type of Fermi liquid of composite fermions (CF's), which are electrons with two magnetic flux quanta attached to each of them. The effective magnetic field in the mean-field approximation acting on the CF is $\Delta B=B-4\pi\hbar n_s/e$, where n_s is the density of the electrons. The flux quanta cancel out the external magnetic field B at $\nu=\frac{1}{2}$, leading to the appearance of the well-defined Fermi surface.[3] It has been argued that fluctuations of the Chern-Simons gauge field from the mean value may result in a partial breakdown of the Fermi liquid.[3,4]

In this paper, we investigate effects of nonuniform magnetic fields on electronic states in quantum wires. We first consider a case, where the magnetic field is assumed to be nonuniform in the transverse direction, whereas it is uniform in the longitudinal direction. The transport is hence anticipated to be ballistic in this situation. Our calculation is related to a recent experiment,[5] in which ballistic transport of the CF has been investigated in narow crossed-wire junctions. The amplitude of the dip in the bend resistance R_B due to the CF was considerably large despite the fact that the mean free path of the CF was an order of magnitude smaller than that of the electrons.[5] It was also found[5] that the ratio of the widths of the negative resistance dip in magnetic field near $\nu=\frac{1}{2}$ and near $B=0$ was much larger compared to the theoretically[3] expected value of $\sqrt{2}$. These observations suggest that the channel width for the CF's is narrower than that for the electrons. In wires defined by means of lateral depletion, the carrier density decreases gradually near the boundaries of the channel in the transverse direction. Therefore, the CF will feel a finite effective magnetic field near the smooth channel boundaries even when ΔB is adjusted to be zero at the center of the channel.[6,7] The varying effective magnetic field may result in narrowing the effective channel width for the CF. We examine the electronic states in quasi-1D wires in the presence of magnetic fields that are parabolic in the transverse direction. It is found that the transverse wave function is strongly influenced by the magnetic field. We calculate R_B and the Hall resistance R_H in a crossed-wire junction, in which the parabolic magnetic field is assumed. We show that the magnetic fields at which the peak in R_B takes place or $R_H=0$ are shifted due to the parabolic magnetic field and they do not coincide. The shift in B may thus be utilized to deduce the strength of the nonuniform effective magnetic field for the CF.

We then investigate the conductance of quasi-1D wires in the presence of random magnetic fields. Because of the nonlocality of quantum-mechanical propagation of an electron, a weak-localization correction to the conductivity emerges when the phase coherence length exceeds the length scale over which the magnetic field is uniform.[8,9] Effects of a random magnetic field on the electronic states are expected to play an important role in the composite fermion theory of the fractional quantum Hall states.[3,4,10] We study the effects of the scattering from the random magnetic fields in a simple model. The magnetic field is assumed to be randomly modulated in the direction along the wire whereas it is uniform in the transverse direction. The behaviors of the localization length and the conductance fluctuations are examined for

different values of the average magnetic field.

II. ELECTRONIC STATES IN QUANTUM WIRES

Let us first consider a particle in narrow wires defined by a parabolic confinement potential $V(y)=(1/2)m\omega_0^2y^2$, where m is the effective mass of the particle. The effective mass of the CF has been found[11] to increase drastically as $\nu\rightarrow\frac{1}{2}$. However, m is assumed to be independent of magnetic fields throughout this paper. We also assume the presence of a parabolic magnetic field $B(y)=B_0+B_2y^2$. In the semiclassical approximation, the deviation of the carrier density from the value at the center of the channel is $\Delta n(y)=(m/2\pi\hbar^2)V(y)$. Here, we have assumed the spin-polarized 2D density of states. Therefore, the effective magnetic field for the CF may be approximated by the parabolic magnetic field with $B_2=m^2\omega_0^2/\hbar e$. This approximation is valid[6,7] when the length scale of the potential variation is larger than the magnetic length $l_B=(\hbar/eB)^{1/2}$. We have included $B_0=B-B_{1/2}$, where $B_{1/2}=4\pi\hbar n_s/e$. The Hamiltonian is thus given as

$$H=\frac{1}{2m}\left(p_x+eB_0y+\frac{eB_2}{3}y^3\right)^2+\frac{p_y^2}{2m}+\frac{1}{2}m\omega_0^2y^2. \quad (1)$$

The Schrödinger equation for a particle with the Fermi energy E_F is

$$\left[-\frac{d^2}{d\rho^2}+(\kappa+\beta_0\rho+\beta_2\rho^3)^2+\rho^2\right]\varphi(\rho)=\varepsilon\varphi(\rho), \quad (2)$$

where $\rho=(m\omega_0/\hbar)^{1/2}y$, $\kappa=(\hbar/m\omega_0)^{1/2}k$, $\varepsilon=2E_F/\hbar\omega_0$, $\beta_0=eB_0/m\omega_0$, and $\beta_2=\hbar eB_2/3m^2\omega_0^2$. The wave function is given in separable form as $\Psi(x,y)=e^{ikx}\varphi(y)$. The effective potential for the particle incorporating the effect of the magnetic field is

$$V_{\rm eff}(\kappa,\rho)=(\kappa+\beta_0\rho+\beta_2\rho^3)^2+\rho^2. \quad (3)$$

Müller[12] has investigated the effect of an antisymmetric magnetic field and found that the time-reversal symmetry is broken. One can see in Eq. (3) that this symmetry is conserved in our case as we consider the symmetric magnetic field. We expand the transverse wave function $\varphi(\rho)$ in terms of the solutions for $\beta_0=\beta_2=0$, i.e., $\varphi(\rho)=\Sigma c_j\phi_j(\rho)$, where $\phi_j(\rho)$ are the oscillator function. Then, Eq. (2) is reduced to a set of equations:

$$\sum_j\left[(\varepsilon-\kappa^2-2j-1)\delta_{jl}-2\kappa\beta_0\langle\rho\rangle_{jl}-\beta_0^2\langle\rho^2\rangle_{jl}-2\kappa\beta_2\langle\rho^3\rangle_{jl}-2\beta_0\beta_2\langle\rho^4\rangle_{jl}-\beta_2^2\langle\rho^6\rangle_{jl}\right]c_j=0, \quad (4)$$

where

$$\langle\rho^s\rangle_{jl}=\int_{-\infty}^{\infty}H_j(\rho)\rho^sH_l(\rho)e^{-\rho^2}\,d\rho, \quad (5)$$

with $H_j(\rho)$ being the Hermite polynomials.

For the CF, we obtain $\beta_2=\frac{1}{3}$ within the above-mentioned approximation. However, we shall consider β_2 as a parameter in the following discussion. In Fig. 1, the band-edge energies, i.e., ε_n for which $\kappa_n=0$, are plotted as a function of the magnetic field β_2. We show the results when $\beta_0=-1$, 0, and 1, which correspond to cases for the CF when the filling factor at the center of the channel is $\nu>\frac{1}{2}$, $\nu=\frac{1}{2}$, and $\nu<\frac{1}{2}$, respectively. Equation (2) is exactly solvable[13] when $\beta_2=0$ with the solution $\varepsilon_n^0=(1+\beta_0^2)^{1/2}(2n+1)$. The corrections to the nth threshold energy up to the order of β_2^2 are obtained as

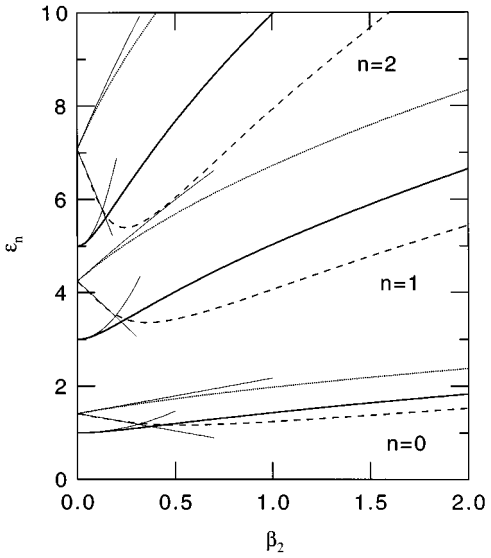

FIG. 1. Threshold energy ε_n of the lowest three subbands as a function of β_2. The values of β_0 for the solid, dotted, and dashed lines are 0, 1, and -1, respectively. The thin solid lines show results of the perturbation calculation.

$$\varepsilon_n=\varepsilon_n^0+\frac{\beta_0\beta_2}{1+\beta_0^2}F_1(n)+\frac{\beta_2^2}{(1+\beta_0^2)^{3/2}}F_2(n)-\frac{\beta_0^2\beta_2^2}{(1+\beta_0^2)^3}F_3(n), \quad (6)$$

where $F_1(n)=(3/2)(2n^2+2n+1)$, $F_2(n)=(5/8)(4n^3+6n^2+8n+3)$, and $F_3(n)=(1/4)(34n^3+51n^2+59n+21)$. The result of the perturbation calculation is shown in Fig. 1 by thin solid lines. The subband edge is increased in energy by the magnetic field compared to the zero-field case. This can be interpreted to mean that the effective channel width for the CF gets narrower than that for the electrons due to the varying magnetic field. When $\beta_0\beta_2<0$, both positive and negative magnetic-field regions are present in the wire. In this situation, the subband energy is found to take a minimum value at finite β_2 though the minimum value is still larger than the subband energy in the absence of magnetic field. The value of κ_n^2 is shown in Fig. 2 for $\varepsilon=6$. At $\beta_0=\beta_2=0$, $\kappa_n^2=\varepsilon-(2n+1)$. We find numerically that the wave vector is either purely real or purely imaginary,[14] and so $\mathrm{Im}\kappa_n^2=0$. Magnetic depopulation of the subband takes place when $\kappa_n^2=0$.

The transverse wave function of the lowest four subbands for $\varepsilon=6$, $\beta_0=0$, and $\beta_2=0.5$ is shown in Fig. 3. Although the magnetic field is zero at the center of the channel, the wave functions shifts towards the right-hand side due to Lorentz force for the positive values of κ_n as obviously seen for the lowest subband. In the parabolic magnetic field, Lorentz

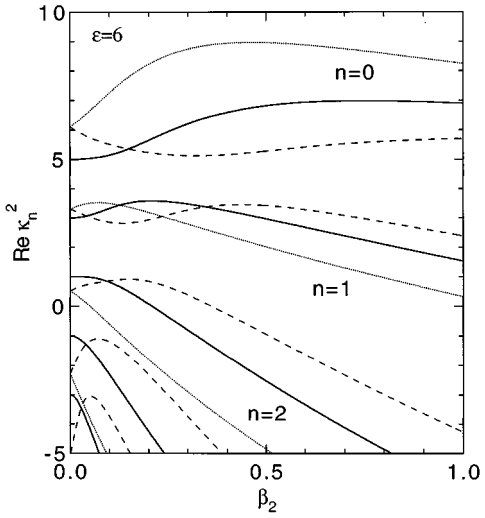

FIG. 2. Values of the real part of κ_n^2 as a function of β_2. The imaginary part is zero. The values of β_0 for the solid, dotted, and dashed lines are 0, 0.5, and -0.5, respectively.

force gets stronger as the electron is pushed further away from the center of the channel. The confinement is, however, imposed because of the parabolic potential. For $\beta_0\beta_2 \leq 0$, the magnetic field becomes zero at $\rho = \pm(-\beta_0/3\beta_2)^{1/2} = \pm\rho_0$. The direction of the Lorentz force is, therefore, reversed around the center of the channel and near the boundaries. The variation of the wave function of the lowest mode when β_0 is varied is shown in Fig. 4. For $\beta_0 < 0$, the probability distribution around the center of the channel is shifted to the negative direction of ρ by the reversed magnetic field as illustrated in the inset of Fig. 4, creating a second peak in the vicinity of $\rho = -\rho_0$. The second peak corresponds to the trajectories confined about the region where $B(x) = 0$ discussed by Müller.[12] The two peaks become comparable in amplitude when $\beta_0 \sim -0.5$. The peak at negative ρ eventually becomes dominant when β_0 is further decreased as the magnetic field in the region where the particle is present becomes entirely negative.

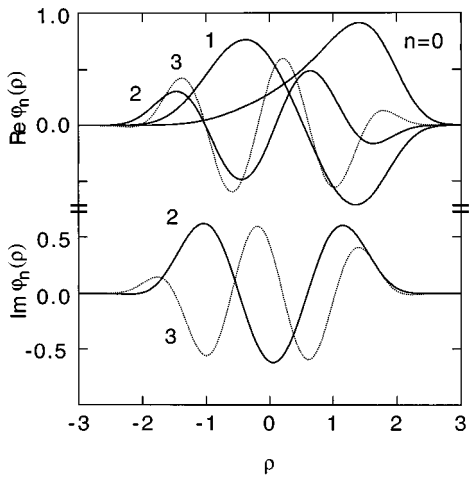

FIG. 3. Transverse wave function of the lowest four subbands for $\varepsilon = 6$, $\beta_0 = 0$, and $\beta_2 = 0.5$. The imaginary part is zero for the propagating modes ($n = 0$ and 1).

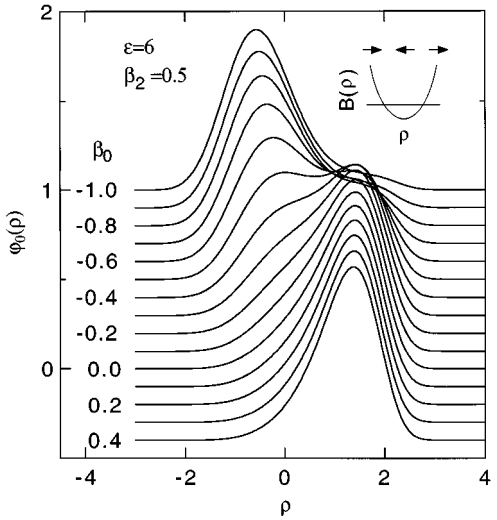

FIG. 4. Transverse wave function of the lowest subband for different values of β_0. Curves are offset for clarity. Inset: The direction of Lorentz force, indicated by the arrows, changes across the channel when $\beta_0\beta_2 < 0$.

The position of the peaks ρ_{peak} and the width $\Delta\rho$ of the wave function at 10% of the maximum are plotted in Fig. 5. As the parabolic magnetic field is applied, the peak position is significantly shifted even when β_2 is small. The distribution initially becomes broader due to the large shift of the peak position. When $\beta_2 > 0.4$, ρ_{peak} is nearly independent of β_0 and gradually approaches zero as the wave vector is suppressed in the large magnetic field. For the large β_2, $\Delta\rho$ is smaller than that in the zero magnetic field, indicating that the probability distribution is squeezed by the magnetic field.

III. TRANSMISSION IN CROSS JUNCTIONS

In relation to the experiment[5] of the negative bend resistance phenomena of the CF, it should be mentioned that the calculation in the previous section deals with the distribution

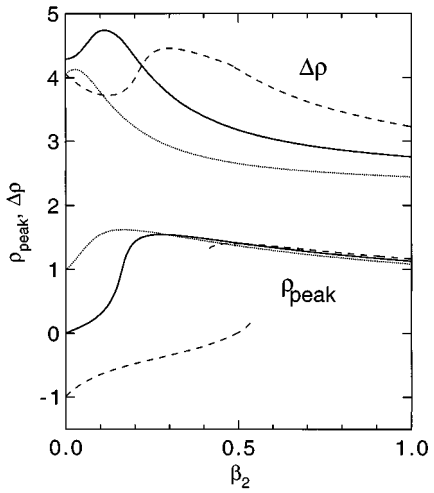

FIG. 5. Position of the peaks ρ_{peak} and the width of the wave function at 10% of the maximum $\Delta\rho$ as a function of β_2 for $\beta_0 = 0.0$ (solid line), 0.5 (dotted line), and -0.5 (dashed line).

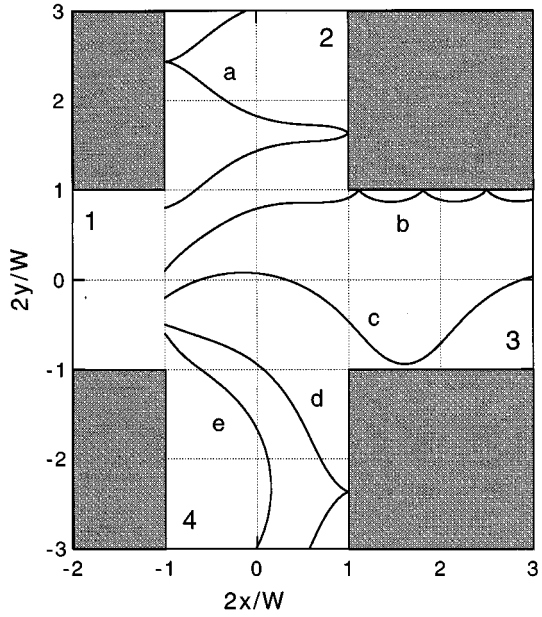

FIG. 6. Typical classical orbits in a cross junction in the parabolic magnetic field when $B_0B_2<0$. Skipping orbit (b), snake orbit (c and e), and traversing orbit (a and d). Four leads are labeled 1–4.

of the injected carriers into the cross region. Ballistic trajectories in the cross region are also altered by the varying magnetic field. This will seriously affect the magnetic-field dependence of the negative bend resistance. The localization of trajectories about the line where the magnetic field is zero may enhance the forward transmission in the cross geometry. In this section, we investigate the four-terminal resistances in narrow crossed-wire junctions in the presence of the nonuniform magnetic field.

Consider a cross junction of straight wires shown in Fig. 6. We divide the crossed-wire junction into four regions and assume the presence of a parabolic confinement potential

$$V(x,y)=\begin{cases} E_F\left(\dfrac{2y}{W}\right)^2, & |x|\geq|y|, \\ E_F\left(\dfrac{2x}{W}\right)^2, & |x|<|y|, \end{cases} \tag{7}$$

and a parabolic magnetic field

$$B(x,y)=\begin{cases} B_0+B_2y^2, & |x|\geq|y|, \\ B_0+B_2x^2, & |x|<|y|. \end{cases} \tag{8}$$

Here, W is the width of the wire at the Fermi energy E_F. The bend resistance R_B and the Hall resistance R_H in the symmetric cross junction are given in terms of the transmission probabilities as

$$R_B=\frac{V_{2\to3}}{I_{1\to4}}=\frac{h}{2e^2}\,\frac{T_LT_R-T_F^2}{(T_L+T_R)\{(T_F+T_L)^2+(T_F+T_R)^2\}}, \tag{9}$$

$$R_H=\frac{V_{4\to2}}{I_{1\to3}}=\frac{h}{2e^2}\,\frac{T_R-T_L}{(T_F+T_L)^2+(T_F+T_R)^2}, \tag{10}$$

where T_L, T_F, and T_R are the transmission probabilities into the left, front, and right probes, respectively. We have employed the billiard model[15] and the lattice Green's-function technique[16,17] to calculate the transmission probabilities.

In the billiard model, the electrons are injected from a lead into the cross region and the transmission probabilities are obtained by counting the number of classical trajectories absorbed by each lead. As we have shown in the prevoius section, the probability distribution for the injection of the carriers into the cross region cannot be easily obtained in the presence of the parabolic potential and the nonuniform magnetic field. Therefore, we have assumed that the cross region of the width and the length W is connected to uniform leads of a square-well confinement potential and $B=0$. This allows us to use simple analytic distribution functions for the injection of the carriers. The abrupt change of the potential and the magnetic field does not scatter the carriers in the classical calculation, and so the results, at least qualitatively, do not depend on this particular choice of the injection.[15] Some of the characteristic trajectories when $B_0B_2<0$ are plotted in Fig. 6. The curves c and e indicate localized trajectories around one of the $B=0$ lines that correspond to the peak near $-\rho_0$ in Fig. 4, whereas the curve b represents the edge state corresponding to the peak at $\rho>0$ in Fig. 4.

The transmission probabilities and R_B are plotted as a function of the offset magnetic field B_0 in Figs. 7(a) and 7(b), respectively. In the absence of the parabolic magnetic field, the diameter of cyclotron orbits $2\hbar k_F/eB_0$ becomes less than the width of the wire when $eW|B_0|\hbar k_F>2$, and so $T_F\approx T_L\approx0$ and R_B disappears in the high magnetic field. With increasing B_2, the position of the maximum forward transmission in B_0 deviates from zero. However, this shift of the forward transmission peak is less reflected in the shift of the dip in R_B. We find that a significant number of carriers are backscattered near $B_0=0$ when $B_2\neq0$. The increase of T_B is effectively equivalent to reducing the number of transmission channels. Consequently, the suppression of the amplitude of the dip in R_B near $B_0=0$ is less pronounced. Nevertheless, the dip in R_B is shifted to negative values of B_0 as B_2 is increased. The vanishing R_H takes place when $T_L=T_R$. Therefore, the positions in B_0 for the dip in R_B and for $R_H=0$ generally do not coincide.

We have also calculated the quantum-mechanical transmission probabilities using the lattice Green's-function technique. The cross junction is simulated by a square lattice and the magnetic field is incorporated in the form of the Pierls' phase factor in the nearest-neighbor hopping elements. The vector potential that we have employed to describe the nonuniform magnetic field is given in the Appendix. The results of the fully quantum-mechanical calculation is shown in Fig. 8. In this calculation, the potential enegy outside the wire of width W is taken to be infinitely large. Similar to the classical calculation, the dip in R_B shifts to lower B_0 as B_2 is increased. In high magnetic fields, R_B becomes zero and quantum Hall plateaus are developed in R_H. It is again found tht the dip in R_B does not coincide with the vanishing of R_H.

Our results show that the parabolic magnetic field in the junction of straight wires lead neither to the enhancement of the peak amplitude in R_B nor to the broadening of the peak in magnetic field, which have been observed in the

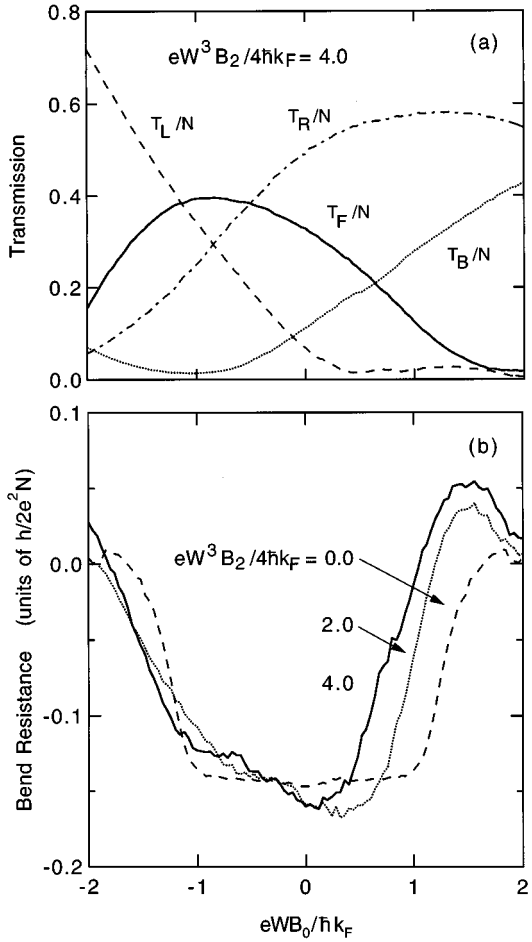

FIG. 7. (a) Transmission probabilities and (b) bend resistance in cross junction as a function of the strength of the uniform magnetic field B_0 calculated by classical model.

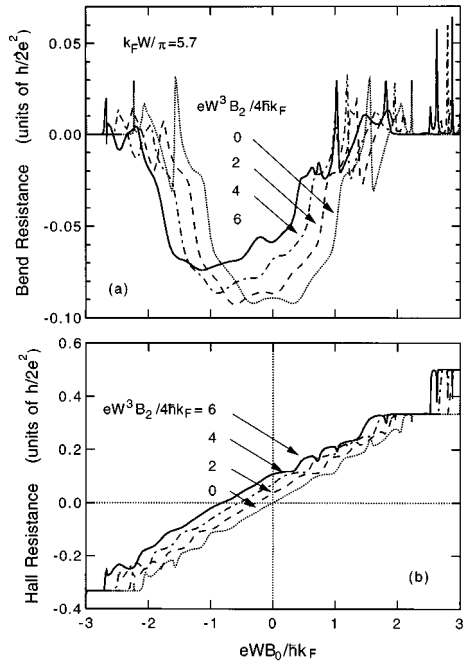

FIG. 8. Results of quantum-mechanical calculation of (a) bend and (b) Hall resistances in cross junction.

experiment.[5] It should be mentioned, however, that the carriers suffer from considerable scattering due to the abrupt change of the magnetic field at $|x|=|y|$ as we have not taken into account the rounded geometry near the corners of the junction. When the incident angle relative to the $B=0$ line is large, the carriers cannot be trapped by the snake orbit[7,12] as shown by the curves *a* and *d* in Fig. 6. The presence of the rounded geometry, and the resulting forward collimation effect, has been shown to be important for the quenching of the low-field Hall resistance.[15,16,18] If the width of the channel widens gradually, as is the case in real samples, the guiding of the trajectories and the forward collimation may be enhanced.

IV. LOCALIZATION AND CONDUCTANCE FLUCTUATIONS IN RANDOM MAGNETIC FIELDS

Quantum interference of scattering from random potentials, such as due to impurities[19,20] and boundary roughness,[21] has been demonstrated to result in universal conductance fluctuations and localization of electronic states. The perturbation calculation[22] in the weak disorder limit has revealed that the magnitude of the conductance fluctuations is universal and on the order of e^2/h. The exact amplitude of the fluctuations depends on universality class for the symmetry of systems. Compared to the zero-magnetic-field case, the fluctuation is suppressed by $1/\sqrt{2}$ (if spin-orbit scattering is absent) in the presence of a magnetic field as time-reversal symmetry is broken. The localization effect is also suppressed in magnetic fields.[19,23] The removal of time-reversal symmetry has been shown to double the localization length ξ in quasi-1D system in the absence of spin-orbit interaction.[24]

We consider a quasi-1D wire with a uniform width W in the presence of a nonuniform magnetic field $B(x)$ perpendicular to the strip. For simplicity, the wire is decomposed into a series of sections with an identical length D and the magnetic field is assumed to be uniform in each section. The magnetic field in section n is chosen as $B_n=B_{\rm av}+\delta B_n$, where δB_n distributes uniformly within an interval to satisfy $\hbar(e|\delta B_n|/m)/E_F<\Delta$. To calculate the conductance of the system, semi-infinite perfect leads with $B(x)=0 (x<0$ and $x>L)$ are attached to the ends of the disordered wire with the total length $L=n_{\max}D$. We choose the gauge such that the vector potential $\mathbf{A}(x,y)=[0,A_y(x),0]$ is given as follows

$$A_y(x)=\begin{cases} 0, & x<0 \\ B_n\{x-(n-1)D\}+D\sum_{i=1}^{n-1} B_i, & (n-1)D<x<nD \\ D\sum_{i=1}^{n_{\max}} B_i, & x>L. \end{cases} \tag{11}$$

When the average magnetic field $B_{\rm av}$ is not zero, finite waveguide segments are inserted between the disordered wire and the perfect leads, in which the magnetic field is graded from

$B_{\rm av}$ to zero. The dimensionless conductance g of the system is given by the Landauer formula

$$g=\sum_{m,n}(v_m/v_n)T_{mn}, \tag{12}$$

where v_m is the velocity of the mode m. The transmission coefficient T_{mn} is obtained from the Green's function using a method based on the one employed by Ando.[17]

We employ the tight-binding model with the site separation a. Each uniform magnetic-field section is represented by $M\times N$ lattice sites. In the following simulations, we choose the sample size to be $M=40$ and $N=10$. Two modes are assumed to be occupied below the Fermi energy when $B=0$ ($k_F W/\pi=2.7$). The second subband is magnetically depleted when $\beta=\hbar(eB_{\rm av}/m)/E_F=0.65$. We restrict the simulation to a regime where the magnetic field is considerably smaller than the depletion threshold. The correlation length of the random magnetic field is thus smaller than the cyclotron radius, and so electrons feel short-range disorder. We have taken the average over 50 samples. The parameters are chosen such that $\lambda_F/a\approx 30$ and the magnetic flux threading through a unit cell is, at the maximum, 0.1% of the magnetic flux quantum h/e, and so we expect that our conclusion remains unchanged in the continuum limit $a\to 0$.

It has been suggested that all states in two dimensions are localized in a random magnetic field with zero average.[2] According to the random-matirx theory, the conductance of an N_c-channel elastic scattering system is obtained as[25]

$$g=\sum_{i=1}^{N_c}\frac{4}{\cosh(\nu_i)+1}, \tag{13}$$

where $\nu_i=2L/\xi_i$. When the localization is strong, where $1\ll\nu_1\ll\nu_2\ll\cdots\ll\nu_N$, we expect $g\propto\exp(-\nu_1)\propto\exp(-2L/\xi)$. The average conductance $\exp(\langle\ln(g)\rangle)$ is plotted in Fig. 9 as a function of the length L of the wire. After the initial rapid decay, the conductance decreases with a single exponential decay constant as the length becomes longer than the localization length ξ. The localization is obviously enhanced as Δ is increased. Analytical calculations using the random-matrix theory[24] and numerical simulations assuming random impurities[19,23] indicate that ξ increases with increasing magnetic field. However, the localization length deduced from the slope becomes smaller when $B_{\rm av}$ is increased as shown in the inset of Fig. 9. Therefore, the effect of the random magnetic field becomes significant as $B_{\rm av}$ deviates from zero. This may be partly due to a reduction of the elastic mean free path l_e in higher magnetic fields[23] since $\xi\approx N_c l_e$ (Ref. 26). It is suggested that δB is not an appropriate parameter to measure the disorder for different values of $B_{\rm av}$.

The root-mean-square deviation of the conductance is shown in Fig. 10. In the weak disorder regime, the amplitude of the fluctuations is found to be universal at $\Delta g=0.3$–0.4 (corresponding to the conductance fluctuations $\sim 0.7e^2/h$), in agreement with the perturbation calculation for impurity scattering in the absence of a magnetic field. The fluctuation is reduced when the average conductance becomes considerably smaller in the localized regime. Because of the limited number of samples, it is not clear if the suppression of the fluctuations due to breaking time-reversal symmetry takes place in the present simulation. We find that the distribution of $\ln(g)$ is well described by a Guassian. The variance of $\ln(g)$ is plotted in Fig. 11. It has been suggested that the variance of $\ln(g)$ in general disordered systems is given in the limiting case as $\mathrm{var}[\ln(g)]\propto(L/l_e)^\gamma$ with $\gamma=2$ or 1 for $L\ll l_e$ or $L\gg l_e$, respectively.[27] However, we find $\gamma\propto 1.8$, which is in between the two limiting values, over the entire range of L irrespective of Δ and $B_{\rm av}$.

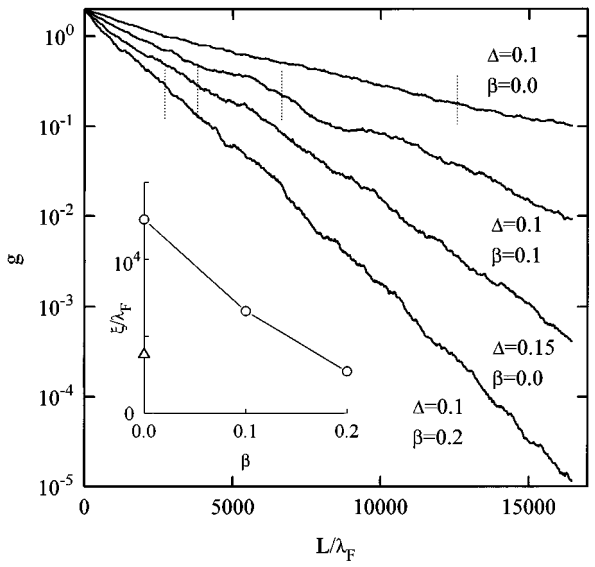

FIG. 9. Average conductance $\exp[\ln(g)]$ as a function of the length L of the wire. The verticle bars indicate the localization lengths. In the inset, the localization length ξ is plotted as a function of the average magnetic field $\beta=\hbar(eB_{\rm av}/m)/E_F$ for $\Delta=0.1$ (circles) and 0.15 (triangle).

V. CONCLUSIONS

In conclusion, we have calculated the electronic subbands in quantum wires in the presence of parabolic magnetic

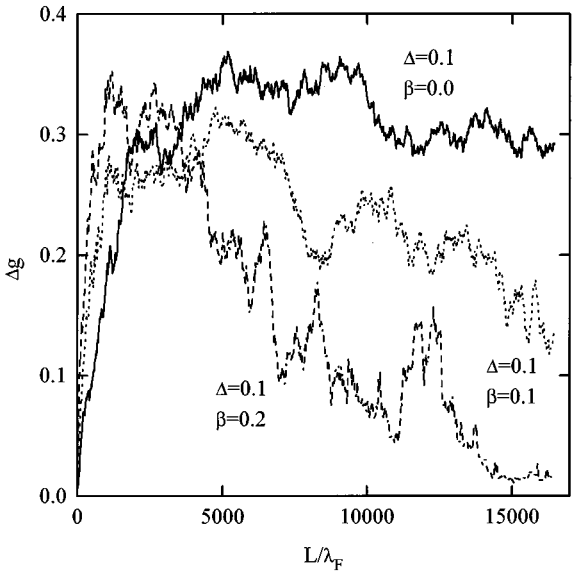

FIG. 10. Root-mean-square deviation of the conductance, $\Delta g=[(g-\langle g\rangle)^2]^{1/2}$, as a function of the length L of the wire.

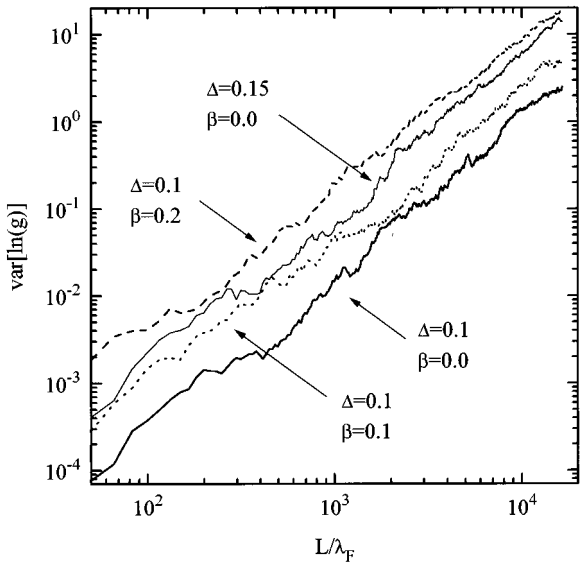

FIG. 11. Variance of $\ln(g)$ as a function of the length L of the wire. The fluctuation increases as $\mathrm{var}[\ln(g)]\propto L^{\gamma}$ with $\gamma\approx 1.8$.

fields. For a parameter expected to be relevant to the composite fermions (i.e., $\beta_2\approx\frac{1}{3}$), the probability distribution is squeezed in the transverse direction and the threshold energy is increased compared to the zero-magnetic-field value. These findings indicate that the effective channel width for the composite fermions is narrower than that for the electrons if the simple model of the varying effective magnetic field we have employed here is reasonable. If the quantized conductance of the composite fermions is observed, the shift in the threshold energy due to the unbalanced magnetic field will be of significant importance. When a negative offset magnetic field is imposed, the wave function can have two peaks: one near the channel boundary and the other near the boundary between positive and negative magnetic field regions. As the double peak does not appear when a positive offset is added, the magnetoresistance of the composite fermions in narrow wires is expected to be asymmetric with respect to $\nu=\frac{1}{2}$. We have confirmed this by the classical and the quantum-mechanical calculations of the four-terminal resistances in a crossed-wire junction. It is indicated that the shape of the negative bend resistance dip is modified in the presence of the parabolic magnetic field. The deviations of the positions of the dip of the bend resistance and the vanishing Hall resistance in magnetic field can be utilized to probe the varing effective magnetic field for the composite fermions. In addition to the nonuniform magnetic field due to variation of carrier density in confined systems, the composite fermion experiences random magnetic fields due to the Chern-Simons gauge field. We have numerically calculated the conductance of quasi-one-dimensional wires in the presence of one-dimensional random magnetic fields. The effect of the fluctuation of the magnetic field becomes significant as the average magnetic field is increased.

ACKNOWLEDGMENT

This work was supported in part by the Bundesministerium für Forschung und Technologie of the Federal Republic of Germany.

APPENDIX

We compute the quantum transmission probabilities using the lattice Green's-function technique. We simulate the sample by a square lattice with the site separation a. The Schrödinger equation is reduced to a tight-binding Hamiltonian for a square lattice with nearest-neighbor interactions:

$$H=\sum \varepsilon_i|i\rangle\langle i|+\sum_{\text{n.n.}} U_{ij}|i\rangle\langle j|, \tag{A1}$$

where the on-site energy at the site $i=(m,n)$ is $\varepsilon_i=-4t$ with $t=-\hbar^2/2ma^2$. In the presence of the magnetic field, the hopping elements U_{ij} are given by

$$U_{ij}=t\exp\left(-ie\int \mathbf{A}\,dl/\hbar\right). \tag{A2}$$

The required elements of the Green's function are calculated using the recursive technique based on the Dyson equation:

$$G=G_0+G_0VG=G_0+GVG_0, \tag{A3}$$

where the Green's function G of a system in the presence of a perturbation V is related to the Green's function G_0 in the absence of V. In the perfect lead, the wave function $u_n(q)$ of the nth mode is given by

$$u_n(q)=C_n\exp(ieAqa/\hbar)\sin[n\pi q/(M+1)], \tag{A4}$$

where M is the number of the sites in the transverse direction, i.e., $W=(M+1)a$. We have assumed the presence of a constant vector potential $\mathbf{A}=(0,A,0)$. The normalization coefficient C_n is

$$C_n=\left[\frac{M}{2}+\frac{1}{2}\,\mathrm{Re}\left(\frac{1-e^{i2\pi nM/(M+1)}}{1-e^{-i2\pi n/(M+1)}}\right)\right]^{1/2}. \tag{A5}$$

The wave vector k_n in the x direction is given by

$$2t[1-\cos\{n\pi/(M+1)\}]+2t[1-\cos(k_na)]=E_F. \tag{A6}$$

The velocity of the mode m is given as $\nu_m=\sin(k_ma)$.

In the remainder of this Appendix, we describe the vector potential $\mathbf{A}$ that we have employed in our simulation of the cross junction. The parabolic magnetic field in the symmetric cross junction given by Eq. (8) can be represented by the vector potential:

$$\mathbf{A}(x,y)=\begin{cases}(-\frac{1}{2}B_0y-\frac{1}{4}B_2y^3,\frac{1}{2}B_0x+\frac{1}{4}B_2xy^2,0), & |x|\geqslant|y|\\ (-\frac{1}{2}B_0y-\frac{1}{4}B_2x^2y,\frac{1}{2}B_0x+\frac{1}{4}B_2x^3,0), & |x|<|y|.\end{cases} \tag{A7}$$

Generally, the transmission coefficients are obtained from the Green's function. However, the relation between the transmission coefficients and the Green's function is not simple in the presence of the magnetic field. Moreover, one needs to know the Green's function of semi-infinite leads, in which the vector potential is given by Eq. (20), for the recursive calculation. This is obviously not easily calculated. In the absence of the magnetic field, the transmission coefficients are simply given as a projection of the Green's function onto the transverse wave function. Therefore, we terminate the

cross junction by semi-infinite leads, in which $B=0$. Contrary to the classical case, the abrupt change of the magnetic field results in quantum-mechanical reflection. To suppress the scattering at the interface, we insert waveguide sections between the cross junction and the $B=0$ leads, in which the magnetic field is graded from the value in the cross junction to zero. In the following, we focus on the vector potential in the lead 3 in Fig. 6. The vector potential in other leads is similarly obtained. We assume that the magnetic field decreases linearly in the lead with the length l attached to the cross junction at $x=d$, i.e., $B(x,y)=(B_2y^2+B_0)(d+l-x)/l$. The vector potential to describe this magnetic field is

$$\mathbf{A}(x,y)=\left[-\left(\frac{1}{2}B_0+\frac{1}{4}B_2y^2\right)y\frac{d+l-x}{l},\right.$$
$$\left.-\left(\frac{1}{2}B_0+\frac{1}{4}B_2y^2\right)y\frac{x(x-2d-2l)+d^2}{2l},0\right]$$
$$(d\leqslant x\leqslant d+l). \quad \text{(A8)}$$

One finds that the vector potential in the zero-magnetic-field lead is not zero and is given as

$$\mathbf{A}(x,y)=\left[0,\left(\frac{1}{2}B_0+\frac{1}{4}B_2y^2\right)\left(d+\frac{l}{2}\right),0\right] \quad (x\geqslant d+l). \quad \text{(A9)}$$

The wave function of the nth mode in the semi-infinite lead, which is necessary to calculate the Green's function, is given using the Gauge transformation as

$$\Psi_n(x,y)=\exp\left[-i\frac{e}{\hbar}\left(d+\frac{l}{2}\right)\left(\frac{1}{2}B_0+\frac{1}{12}B_2y^2\right)y\right]e^{ik_nx}u_n(y)$$
$$(x\geqslant d+l), \quad \text{(A10)}$$

where $e^{ik_nx}u_n(y)$ is the wave function when $\mathbf{A}=0$.

[1] B. L. Altshuler and L. B. Ioffe, Phys. Rev. Lett. **69**, 2979 (1992); T. Sugiyama and N. Nagoasa, *ibid.* **70**, 1980 (1993); S.-C. Zhang and D. P. Arovas, *ibid.* **72**, 1886 (1994).
[2] D. K. K. Lee and J. T. Chalker, Phys. Rev. Lett. **72**, 1510 (1994).
[3] B. I. Halperin, P. A. Lee, and N. Read, Phys. Rev. B **47**, 7312 (1993).
[4] Y. B. Kim, A. Furusaki, X.-G. Wen, and P. A. Lee, Phys. Rev. B **50**, 17 917 (1994); Y. B. Kim, P. A. Lee, X.-G. Wen, and P. C. E. Stamp, *ibid.* **51**, 10 779 (1995).
[5] J. Herfort, Y. Takagaki, R. Hey, K.-J. Friedland, K. H. Ploog, D. K. Maude, J. C. Portal, J. Takahara, and K. Gamo (unpublished).
[6] L. Brey, Phys. Rev. B **50**, 11 861 (1994).
[7] D. B. Chklovskii and P. A. Lee, Phys. Rev. B **48**, 18 060 (1993); D. B. Chklovskii, *ibid.* **51**, 9895 (1995).
[8] J. Rammer and A. L. Shelankov, Phys. Rev. B **36**, 3135 (1987).
[9] S. J. Bending, K. v. Klitzing, and K. Ploog, Phys. Rev. Lett. **65**, 1060 (1990); A. Smith, R. Taboryski, L. T. Hansen, C. B. Sørensen, P. Hedegård, and P. E. Lindelof, Phys. Rev. B **50**, 14 726 (1994).
[10] J. K. Jain, Phys. Rev. Lett. **63**, 199 (1989).
[11] R. R. Du, H. L. Stormer, D. C. Tsui, A. S. Yeh, L. N. Pfeiffer, and K. W. West, Phys. Rev. Lett. **73**, 3274 (1994).
[12] J. E. Müller, Phys. Rev. Lett. **68**, 385 (1992).
[13] S. B. Kaplan and A. C. Warren, Phys. Rev. B **34**, 1346 (1986); K. -F. Berggren, G. Roos, and H. van Houten, *ibid.* **37**, 10 118 (1988).
[14] R. L. Schult, H. W. Wyld, and D. G. Ravenhall, Phys. Rev. B **41**, 12 760 (1990).
[15] C. W. J. Beenakker and H. van Houten, Phys. Rev. Lett. **63**, 1857 (1989).
[16] H. U. Baranger, D. P. DiVincenzo, R. A. Jalabert, and A. D. Stone, Phys. Rev. B **44**, 10 637 (1991).
[17] T. Ando, Phys. Rev. B **44**, 8017 (1991).
[18] H. U. Baranger and A. D. Stone, Phys. Rev. Lett. **63**, 414 (1989).
[19] P. A. Lee and S. Fisher, Phys. Rev. Lett. **47**, 882 (1981).
[20] A. D. Stone, Phys. Rev. Lett. **54**, 2692 (1985).
[21] Y. Takagaki and D. K. Ferry, J. Phys. Condens. Matter **4**, 10 421 (1992).
[22] P. A. Lee, A. D. Stone, and H. Fukuyama, Phys. Rev. B **35**, 1039 (1987).
[23] H. Tamura and T. Ando, Phys. Rev. B **44**, 1792 (1991).
[24] J. -L. Pichard, M. Sanquer, K. Slevin, and P. Debray, Phys. Rev. Lett. **65**, 1812 (1990).
[25] J. -L. Pichard, and G. André, Europhys. Lett. **6**, 477 (1986).
[26] J. -L. Pichard, in *Quantum Coherence in Mesoscopic Systems*, edited by B. Kramer (Plenum, New York, 1991), p. 369.
[27] A. A. Abrikosov, Solid State Commun. **37**, 997 (1981).